Theoretical and Applied Climatology (2025) 156:437
https://doi.org/10.1007/s00704-025-05664-z

RESEARCH

Analysis of maize drought risk characteristics and dominant risk factors based on crop growth stage in the Yellow River Basin

Ying Wang[1] · Jianshun Wang[1] · Yue Zhou[2]

Received: 11 October 2024 / Accepted: 7 July 2025 / Published online: 29 July 2025

Abstract
The Yellow River Basin is a major agricultural production area in China, and the security of maize production in this region is of strategic importance for ensuring national food security. This study constructs a drought disaster risk evaluation index system for the maize growth stages and integrates the Optimal Parameter-based Geographical Detector (OPGD) model to systematically analyze the spatiotemporal heterogeneity patterns and dominant risk factors of maize drought risk in the Yellow River Basin. Results indicate that high-hazard areas of drought disaster are primarily distributed in the upper reaches of the Yellow River, exhibiting a contracting trend from southeast to northwest from the sowing-to-emergence stage (G1) to the milk-ripening-to-maturity stage (G5). The high-exposure areas are concentrated in the irrigated zones along the Yellow River (Ningxia Plain, Hetao Irrigation District, Guanzhong Plain, and downstream irrigated areas). The high-vulnerability areas are centered on the Ningxia Plain and Northern Shaanxi Plateau, with vulnerability peaking during the emergence-to-jointing stage (G2). The high-sensitivity areas are located in the central-northern part of the middle reaches. During the tasseling-to-milk-ripening stage (G4), sensitivity is highest in the upper/middle reaches, while during the milk-ripening-to-maturity stage (G5), sensitivity is most pronounced in the downstream regions. The high-drought-risk areas are predominantly located in the upper reaches and northern middle reaches, with their spatial extent progressively contracting northwestward as the maize growth stages progresses. Risk peaks occur during G2 in the upper reaches, G1-G2 in the middle reaches, and G1/G5 in the downstream region. OPGD model analysis reveals that risk in the upper reaches is dominated by hazard and vulnerability components, while exposure is the dominant components in the middle and lower reaches. Hazard primarily determines the overall spatial pattern of risk, whereas vulnerability/sensitivity/exposure components shape the localized characteristics. The fine-scale evaluation framework for maize growth stages developed in this study is fundamentally distinct from approaches based on administrative units or macro-scale indicators, offering a scientific basis for customized mitigation strategies in the Yellow River Basin.

1 Introduction

In recent years, the accelerated global warming has exceeded the natural variability of the Earth's climate system over the past several centuries. This has resulted in amplified climate fluctuations, an accelerated hydrological cycle, and increasingly extreme water redistribution. Consequently, extreme weather and climate events—such as droughts, floods, and high temperatures—have become more frequent, intense, and prolonged across many regions globally (Allan 2023). Under this trend, the frequency of 10-year drought events has increased by 1.7 times, with a 0.3 increase in drought indices. At the same time, the frequency of extreme heat events has increased by 2.8 times, with an intensity rise of 1.2°C, causing severe impacts on ecosystems and human societies. (IPCC 2021). Should current emission scenarios

✉ Ying Wang
wangyn924@163.com

[1] Key Laboratory of Arid Climatic Change and Reducing Disaster of Gansu Province, Key Open Laboratory of Arid Change and Disaster Reduction of CMA, Institute of Arid Meteorology, China Meteorological Administration, Lanzhou 730020, Gansu, China

[2] China Meteorological Administration Basin Heavy Rainfall Key Laboratory / Hubei Key Laboratory for Heavy Rain Monitoring and Warning Research, Institute of Heavy Rain, China Meteorological Administration, Wuhan 430205, China

persist, projections indicate a significant reduction in terrestrial water storage within global arid zones by 2100. Concurrently, the extent of arid regions is anticipated to expand by 4.1–10.6%, leading to a continuous escalation in drought disaster risk (Liu et al. 2023). China is situated within the combined influence zone of the East Asian tropical and subtropical monsoons. It is also subject to westerly circulation and the Tibetan Plateau monsoon, resulting in three distinct natural geographical regions: the humid monsoon zone, the inland arid zone, and the Qinghai-Tibetan alpine zone. Constrained by its physiography and climatic conditions, China is severely affected by drought disasters (Wang et al. 2019). Statistically, drought causes an average annual crop loss area of 8.9×10^6 ha in China. Annual grain production reductions range from several million to over 30 million tons, with average direct economic loss reaching 44 billion RMB (Su et al. 2018). Under the backdrop of climate warming, the drought extent is expanding continuously across China, its spatial distribution pattern is shifting markedly, and extreme drought events are increasing significantly (Zhang et al. 2024a). A notable example is the severe meteorological drought in July 2022 within the Yangtze River Basin-the most intense since 1961-which exhibited the rare phenomenon of "drought during the main flood period". Projections indicate that future climate-induced alterations in temperature and precipitation patterns will continue to directly and indirectly reduce crop yields. By 2050, an estimated 300 million people in China could be affected (Chen et al. 2024). Consequently, drought has long been a national priority and remains a central research focus within the scientific community.

The Yellow River Basin, situated in mid-latitudes, spans an arid-to-semi-humid transitional zone. Connecting the Qinghai-Tibet Plateau, Loess Plateau, and North China Plain, it constitutes a vital ecological security barrier for China. The middle-lower reaches of the Yellow River Basin benefit from monsoon climate, characterized by concurrent precipitation and elevated temperatures, along with abundant sunlight, which creates favorable agroclimatic conditions for agriculture. As a traditional agricultural core, this region contains 20.24 million hectares of cropland, contributing approximately one-third of the China's grain output and holding strategic agricultural significance (Liu et al. 2020; Ma et al. 2020). Against climate change, basin-wide temperatures show a consistent upward trend (0.30 °C/decade), while extreme precipitation frequency increases (Ma et al. 2020; Gao et al. 2023). Human water withdrawals now exceed 85% of total surface runoff—surpassing the ecological threshold for healthy rivers (40%) (Ma et al. 2020). Under the combined climatic and anthropogenic pressures, extreme droughts are intensifying in frequency and severity, exacerbating water scarcity and threatening agricultural and water security (Jiang et al. 2023). For example, drought prevented cultivation on 215,400 hectares of Henan Province farmland in 2024, causing minimum verified agricultural losses of 3 billion yuan (RMB). Consequently, as a critical economic corridor of China's Belt and Road Initiative, sustaining the basin's ecological integrity is paramount to national security.

As the disaster prevention paradigm shifts from reactive drought relief to proactive drought prevention, drought management has transitioned from crisis management to a risk management framework. Within this framework, drought risk assessment constitutes the core component of risk management (IPCC 2021). Current research on drought risk characteristics in the Yellow River Basin and its response mechanisms to climate change remains insufficient. Existing studies have primarily focused on drought indices derived from meteorological, hydrological, or remote sensing data to examine the evolution of drought characteristics—including frequency, duration, peak intensity, and severity—across the basin (Wang et al. 2025; Ding et al. 2024). These findings constitute hazard-oriented drought research, addressing direct causative factors in drought disaster formation. They provide critical insights for understanding drought onset/termination timing, frequency, intensity, and spatial extent. However, as drought risk represents a complex systemic phenomenon, comprehensive research must fully account for the roles of exposure and vulnerability in disaster manifestation. Exposure is typically quantified through value-based metrics of assets exposed to drought events, such as population density, agricultural/forest land area, and GDP (Wang et al. 2023a; Xue et al. 2024). Vulnerability assessment typically employs indicator-based approaches tailored to research objectives. For instance, studies have constructed vulnerability evaluation indices using multi-source data—including Visible Infrared Imaging Radiometer Suite (VIIRS) nighttime lights data and Moderate Resolution Imaging Spectroradiometer (MODIS) products—based on a stability-resistance-resilience framework to examine spatiotemporal evolution patterns of terrestrial ecosystem vulnerability in the Yellow River Basin (Zhu et al. 2025; Zhang et al. 2022a). Drought disaster risk emerges from the synergistic interaction of hazard, exposure, and vulnerability. A key research challenge lies in developing scientifically robust risk assessment indicators that account for regional eco-climatic characteristics and elements at risk. Previous studies have established agricultural and ecological drought risk assessment models for the basin (Han et al. 2021; Wang et al. 2023a). These investigations reveal a distinct spatial pattern wherein agricultural drought risk intensifies downstream relative to upstream regions. This gradient is primarily governed by monsoonal climate, complex topography, socioeconomic development levels, population exposure, and water supply-demand imbalances—though the spatial contributions of individual risk factors remain unquantified. Ecological drought high-risk zones concentrate predominantly in the Shaanbei Plateau, Longzhong Plateau, Ningxia Plain, and Hetao Plain (excluding irrigated areas). Upper basin vulnerability demonstrates co-dependence on land surface temperature and precipitation, whereas the Guanzhong Basin (mid-basin) and lower reaches exhibit precipitation-dominated vulnerability. Collectively, these static risk assessments provide foundational insights into the spatial distribution characteristics of drought disaster risk across the Yellow River Basin.

Zea mays L. (maize) constitutes the principal food crop in the Yellow River Basin. It simultaneously serves as essential livestock feed and a critical raw material for food processing, healthcare products, light industry, and chemical manufacturing. Drought-induced yield volatility not only compromises production stability but also propagates to downstream sectors, thereby threatening socioeconomic stability. Consequently, enhancing drought risk management for maize in the Yellow River Basin represents an urgent priority. Primary methodologies for assessing maize drought risk include crop modeling approaches (e.g., AquaCrop and DSSAT-CERES) (Hou et al. 2024), which simulate dynamic crop responses to water stress across phenological stages to quantify yield reduction risks; statistical methods (Zhang et al. 2024b; Liu et al. 2022), which derive risk through historical data modeling; and risk-factor frameworks (Cheng et al. 2024; Han et al. 2021), which integrate hazard, exposure, and vulnerability components to analyze natural-socioeconomic interactions. However, key limitations persist: crop models require site-specific parameter calibration, introducing substantial uncertainty at regional scales while neglecting socioeconomic factors; statistical approaches demand extensive datasets yet exhibit weak mechanistic foundations; and prevailing risk-factor assessments employ predominantly static methodologies that overlook critical phenological variations—for example, the water sensitivity coefficient during tasseling (1.2) significantly exceeding seedling stage values (0.3) (Liu et al. 2022; Singh et al. 2023). It is evident that the current drought disaster risk assessment studies are insufficient to support the development of precise regional risk management strategies. Hence, phenology-based drought risk assessment is essential for advancing maize risk management in the basin. Current research predominantly focuses on spatiotemporal drought patterns or hazard dynamics across growth stages (Wang et al. 2023b; Chen et al. 2023), with limited attention paid to the role of exposure and vulnerability components in risk formation.

Therefore, this study focuses on maize cultivation in the Yellow River Basin, developing a phenology-based drought risk assessment model based on hazard, exposure, and vulnerability components. We identify and characterize drought risk characteristics across growth stages and analyze dominant risk components across different regions. The research novelties lie in: (1) Proposing a raster-scale dynamic drought risk assessment model based on maize growth stages, which resolves the spatial-temporal dynamics of maize drought risk across the Yellow River Basin during the crop growth cycle; (2) Integrating the Objective-specific Probabilistic Geospatial Drought (OPGD) model with factor detector analysis to quantify interaction effects among dominant risk factors at different growth stages, thereby providing evidence-based support for region-specific and stage-specific drought mitigation strategies. These outcomes will advance resilience in maize production systems and inform optimized agricultural water resources management throughout the basin.

2 Data and methods

2.1 Study area

The mainstem of the Yellow River spans approximately 5,464 km, with a drainage area of approximately 795,000 km² that constitutes 8.3% of China's total land area. It traverses nine provinces and autonomous regions: Qinghai, Sichuan, Gansu, Ningxia, Inner Mongolia, Shaanxi, Shanxi, Henan, and Shandong. By the end of 2019, the basin's population reached approximately 160 million, with annual agricultural production accounting for approximately 13.4% of the national total. Topographically, the basin descends from west to east, with elevations decreasing from 4,200 m at the source to ~ 1,000 m in the mid-reach and < 50 m in the lower reach. The Yellow River Basin receives abundant solar radiation (annual sunshine duration: 2,000–3,300 h; total solar radiation: 110–160 kcal/m²), providing rich solar-thermal resources. Precipitation patterns, shaped by the East Asian monsoon and mid-latitude westerlies, exhibit a northwest-to-southeast gradient (annual mean: 160–700 mm), with ~ 70% occurring from June to September. Mean annual temperatures increase from west to east and north to south (−4 to 14 °C), while evaporation averages ~ 1,100 mm annually (peaking at > 2,500 mm; Fig. 1). Dominant loess-derived soils (primary and secondary loess) are characterized by high fertility, loose texture, favorable structure, and efficient water retention-drainage capacity—enhancing nutrient/moisture uptake and thus irrigation efficiency. As a key national grain and energy production base, the basin faces acute water scarcity, with agricultural consumption exceeding 60% of total water supply (Ma et al. 2020).

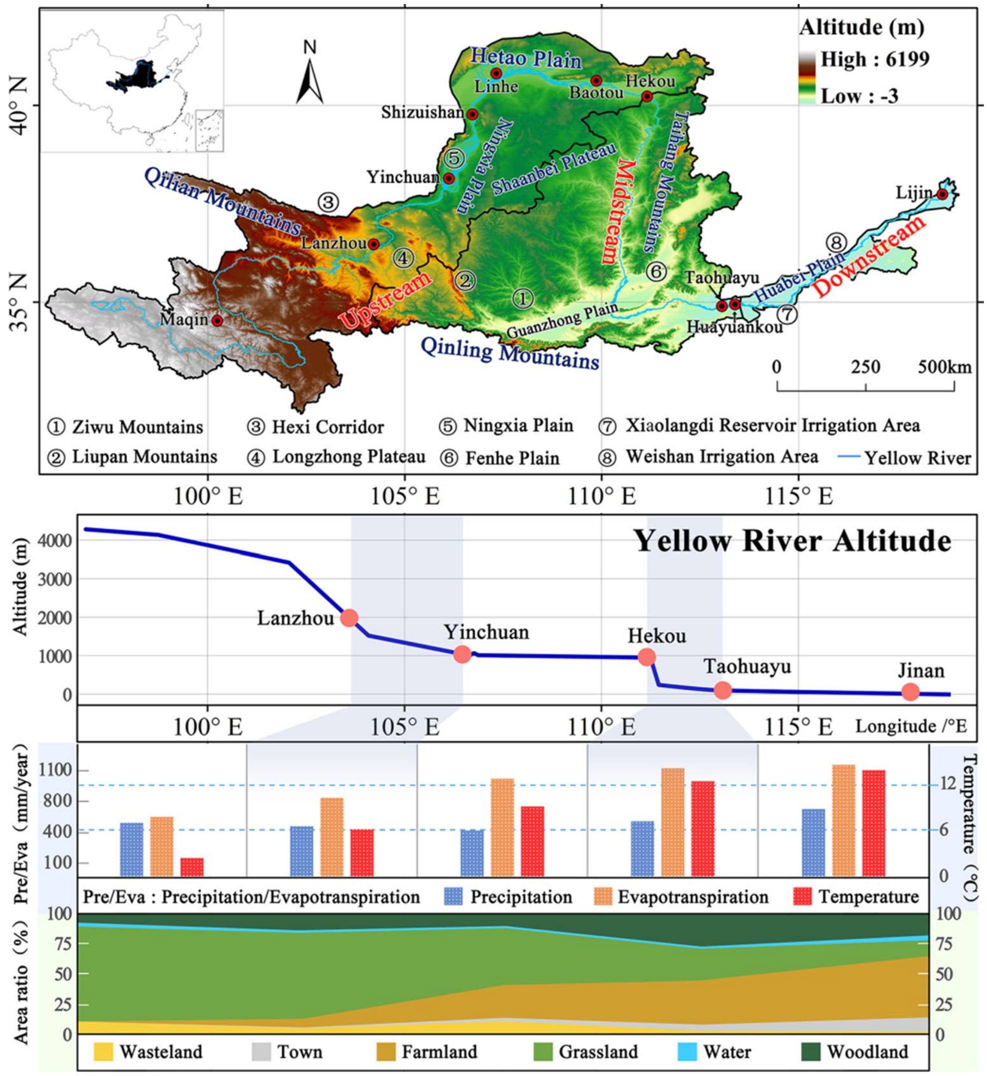

Fig. 1 Location map and characteristics of the Yellow River Basin study area

2.2 Data sources

2.2.1 Meteorological data

Meteorological ground observation data were collected from 250 stations within the maize cultivation zone of the Yellow River Basin from 1960 to 2023 (Fig. 2). Key variables include daily precipitation (mm), mean daily temperature (°C), sunshine duration (h/d), relative humidity (%), and wind speed (m/s). All data were obtained from the National Meteorological Science Data Center (http://data.cma.cn/).

2.2.2 Maize data

Maize yield data (kg/ha) at the grid scale were sourced from the Global Dataset of Annual Yields for Four Major Cereal Crops (Cao et al. 2025). This dataset has a spatial resolution of 5 arc-minutes and an annual temporal resolution, covering the period from 2000 to 2015 (unit: kilograms per hectare, kg/ha; available at: https://doi.org/https://www.nesdc.org.cn/sdo/detail?id=67d157f57e28176b9b452822).

Maize phenological data across the Yellow River Basin were sourced from 54 agrometeorological stations of the China Meteorological Administration (2000–2020), augmented by experimental records from Liu et al. (2021a). Phenophase dates were converted to Day of Year (DOY), with ±2σ outlier years excluded before computing long-term means. Using climate zoning and crop-type classification (spring/summer maize), phenological data were spatially assigned to 250 meteorological stations via nearest-neighbor interpolation (Fig. 2). Validation showed that assigned DOY values across stations resided within literature-reported phenological windows for homologous ecoregions (SD: ±5 days), confirming methodological robustness (Zhang et al. 2015a, b, 2020; Liu et al. 2021b; Ma et al. 2022; Wang et al. 2023c).

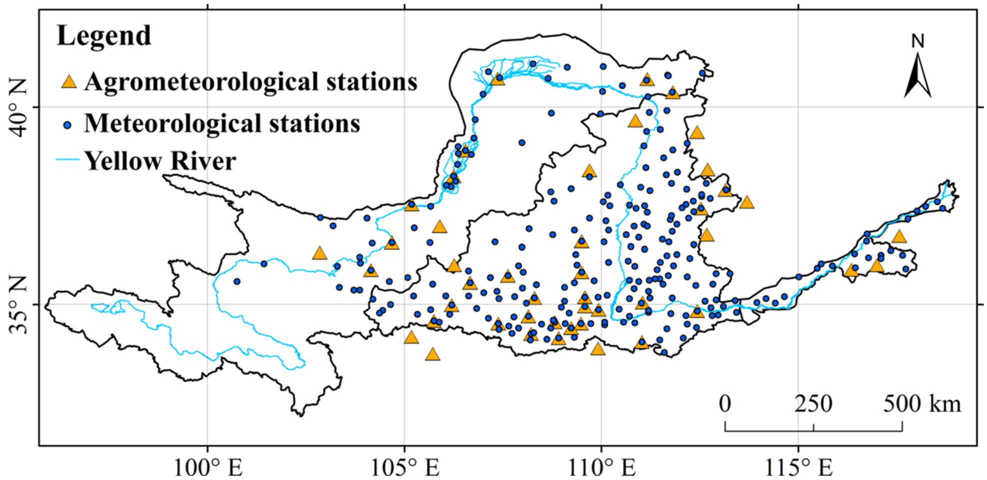

Fig. 2 Map of station distribution in the study area

Table 1 Risk assessment indicators for maize drought in the yellow river basin

	Criterion	Indicators
Disaster-causing factor	Hazard	Frequency and intensity of meteorological drought
Disaster-bearing body	Exposure	multi-year average maize yield per unit area
	Vulnerability	Water demand
Disaster-prone environment	Sensitivity	Irrigation rate Effective precipitation Soil available water content

2.3 Methods

2.3.1 Establishment of a maize drought risk assessment index and model

The risk model applied in this study derives from the IPCC risk framework (IPCC 2023), wherein risk is conceptualized as the synergistic interaction of hazard (H), exposure (E), and vulnerability (V). Building upon disaster system theory (UNDRR 2021), we further decompose vulnerability into two distinct dimensions: disaster-bearing body vulnerability and disaster-prone environment sensitivity. Consequently, a comprehensive indicator system for maize drought risk assessment was developed (Table 1).

2.3.2 Hazard

Drought hazard refers to the risk source, specifically the frequency and intensity of meteorological drought. Because this study is based on maize growth stages, and because the duration and timing of these stages vary significantly across regions, a daily drought index is necessary to identify drought events for determining their frequency and intensity. Analysis of various meteorological drought indicators revealed that the Relative Moisture Index (MI) effectively integrates information on precipitation, temperature, and crop water demand, which allows it to reflect daily-scale atmospheric water balance characteristics, making it an ideal regional drought monitoring indicator (Wu et al. 2021). The calculation equation of MI is as follows (National Standard of the People's RepubLic of China 2017):

$$MI_i = \frac{P_i - PET_i}{PET_i} \tag{1}$$

where MI_i is the relative moisture index on day i, P_i is the precipitation (mm) on day i, and PET_i is the potential evapotranspiration (mm) on day i, calculated using the Penman-Monteith method as recommended by FAO (1979).

During drought onset, when precipitation is absent or persistently below normal, drought conditions progressively develop and intensify. During drought recovery, an effective drought index must exhibit limited sensitivity to precipitation and should avoid drastic fluctuations due to minor precipitation events. Therefore, we optimize the MI index by implementing a time-decaying weighting scheme, where the current-day MI (MI$_1$) contributes most substantially to drought characterization, whereas contributions from prior days diminish with increasing temporal distance. Consistent with Lu (2009), we aggregate MI values over a 30-day backward window. A linearly decreasing weight model is applied with summed weights normalized to unity ($\Sigma = 1$). Let MI$_1$ represent the MI value for the current day, with a weight coefficient of 30/465; MI$_2$ represents the MI value from the previous day, with a weight coefficient of 29/465; and so on, with MI$_{30}$ denoting the MI value from 29 days prior, with a weight of 1/465. The optimized MI index expressed as:

$$MI_{30i} = \sum {}_{i=1}^{30} \frac{i}{465} MI_i \tag{2}$$

Table 2 Classification standard of drought grade based on relative moisture index (MI)

Grade	Drought type	MI
1	None	MI > −0.40
2	Light	−0.65 < MI≤−0.40
3	Moderate	−0.8 < MI≤−0.65
4	Severe	−0.95 < MI≤−0.80
5	Extreme	MI≤−0.95

Based on the conceptualization of hazard drivers in disaster risk theory, we developed a hazard assessment model (Zhang and Wang 2022b):

where MI_{30i} represents the relative moisture index on day i. For the current day, i=30; for the previous day, i=29, and so on, with i=1 corresponding to the data from 29 days prior.

According to the drought severity classification criteria for the MI established in China's National Standard GB/T 20,481−2017—*Meteorological Drought Grade*, the optimized index MI_{30i} is classified as follows:

$$H = \sum {}_{k=1}^{4} (\frac{I_{Ck}}{I_{Cx}} \times P_{Ck}) \tag{3}$$

where H represents the hazard level of disaster-causing factors (%), I_C denotes the intensity level of the disaster-causing factors, which is a non-dimensional number, I_{Cx} is the extreme drought grade value of drought-causing factors, which is a non-dimensional number, k indicates the grade of drought-causing factors (Table 2), and P_{Ck} is the occurrence probability of a disaster-causing factor of drought intensity k, %, calculated using the information distribution method. The information distribution method, a nonparametric estimation approach grounded in fuzzy set theory, operates by transforming crisp sample points within a given dataset into fuzzy sets. This transformation compensates for information gaps in pattern recognition caused by incomplete data (Huang 2012). Detailed computational procedures are documented in (Zhang and Wang 2022b; Huang et al. 2004; Huang 2012).

2.3.3 Exposure

Exposure refers to the extent, quantity, or value of the disaster-bearing body subjected to adverse effects from disaster-causing factors (Qin et al. 2015). Higher exposure indicates greater potential losses in the disaster-bearing body under drought stress. The multi-year average maize yield per unit area is a comprehensive indicator reflecting both land productivity and maize production quality. Therefore, it was selected as the exposure index for drought risk assessment.

2.3.4 Vulnerability

Vulnerability, an inherent attribute of the disaster-bearing body, reflects maize's susceptibility to drought stress and its adaptive capacity. In this study, the crop water demand (WD) during distinct growth stages was selected as the vulnerability index. Maize WD represents the sum of evaporation between plants and leaf transpiration under optimal soil moisture conditions during the growth period, resulting from the interaction of maize's biological traits and environmental factors. Higher WD indicates greater vulnerability to drought, while lower WD implies reduced vulnerability. The equation is formulated as follows:

$$WD_t = PET_t \times K_{ct} \tag{4}$$

where WD is the maize water demand (mm); PET is the reference crop evapotranspiration (mm); K_c is the crop coefficient; and t is the growth period. Crop coefficients (Kc) are provided in Table 3 (National Standard of the People's RepubLic of China 2015; Meteorological Industry Standards of the People's RepubLic of China 2015a, b).

2.3.5 Sensitivity

A disaster-prone environment refers to settings where natural conditions, geographical features, and human activities

Table 3 Crop coefficient (K_c) values of maize at different times

Province/region	Maize type	April	May	June	July	August	September
Qinghai	Spring maize	0.42	0.58	0.8	1.17	1.1	0.84
Gansu	Spring maize	0.42	058	0.8	1.17	1.1	0.84
Ningxia	Spring maize	0.3	0.5	1.26	1.36	1.29	0.69
Inner Mongolia	Spring maize	0.3	0.42	0.71	1.17	1.05	0.72
Shanxi	Spring maize	0.5	0.7	0.8	1.05	0.95	0.6
	Summer maize			0.64	1.14	1.14	0.54
Shaanxi	Spring maize	0.55	0.77	0.785	1.41	1.315	1.17
	Summer maize (east of Guanzhong)			0.51	0.99	1.39	1.86
	Summer maize (west of Guanzhong)			0.51	1.05	1.43	1.28
Henan	Summer maize			0.85	1.32	1.79	1.26
Central Shandong	Summer maize			0.7	1.08	1.5	1.27

collectively create conditions conducive to natural disasters. Such environments typically encompass climatic conditions, topography, soil properties, and vegetation cover. Maize's sensitivity to drought-prone environments reflects the degree to which environmental conditions influence drought transmission to maize crops. This sensitivity is characterized by irrigation rate, effective precipitation, and soil available water content.

The irrigation rate is defined as the ratio of effectively irrigated area to total cultivated land area per unit region. A high irrigation rate indicates that artificial irrigation supplies a greater proportion of agricultural water for maize production, enabling normal growth under natural precipitation deficit.

Effective precipitation refers to the portion of precipitation directly or indirectly available for crop use, including water consumed for essential agricultural processes. This encompasses precipitation utilized through crop interception, plant transpiration, soil evaporation (or water surface evaporation in paddy fields), leaching, and field percolation—all contributing to crop growth and farming operations (Petra and Stefan 2002). It is calculated using the method recommended by the U.S. Department of Agriculture Soil Conservation Service (USDA-SCS) (Smith 1992), with the formula given below:

$$\begin{array}{ll} P_{eff} = \frac{P(4.17-0.2P)}{4.17} & for\ P < 8.3\, mm/\mathrm{day} \\ P_{eff} = 4.17 + 0.1P & for\ P \geq \ 8.3\,\mathrm{mm/day} \end{array} \tag{5}$$

where P_{eff} is the effective precipitation (mm/day) and P is the total precipitation (mm/day).

Soil available water content (AWC) is defined as the difference between field capacity (FC) and permanent wilting point (PWP) in terms of soil water content. This parameter quantifies the soil's capacity to retain and release plant-available water under given conditions, which critically influences crop growth and irrigation management strategies. The equation is expressed as follows:

$$AWC = FC - PWP \tag{6}$$

where FC is the field capacity (cm^3/cm^3) and PWP is the permanent wilting point (cm^3/cm^3).

The drought sensitivity assessment model is:

$$S = \sum {}_{i=1}^{n} X_{Si} W_{Si} \tag{7}$$

where S is sensitivity, X_{Si} is the sensitivity index for the ith factor, W_{Si} is the sensitivity weight assigned to the ith factor, and n is the number of factors. To ensure a fair representation of each factor's contribution to sensitivity across different spatial contexts, each factor is assigned a uniform weight of 1.

2.3.6 Standardization of drought risk assessment indicators

The maize drought risk assessment index system includes multiple indicators with incommensurable units. To ensure comparability among the indicators, normalization is necessary to scale the values within the range of 0 to 1. The calculation equation is as follows:

$$R_{ij} = \frac{X_{ij} - min_j X_{ij}}{max_j X_{ij} - min_j X_{ij}} \tag{8}$$

where R_{ij} is the normalized value of the ith indicator in region J; X_{ij} denotes the original value of the ith indicator in region J; and $max_j X_{ij}$ and $min_j X_{ij}$ represent the maximum and minimum values of the ith index in zone J, respectively.

2.3.7 Maize drought risk assessment model

Within the risk components of maize drought disasters, hazard, exposure, vulnerability, and sensitivity collectively contribute positively to risk formation. Consequently, the drought risk model is formulated as follows:

$$R = H^{W_H} \times E^{W_E} \times V^{W_V} \times S^{W_S} \tag{9}$$

where R is the maize drought risk; H, E, V, and S represent hazard, exposure, vulnerability, and sensitivity, respectively; and W_H, W_E, W_V, and W_S are the respective weights assigned to these factors. To ensure equitable representation of each factor's contribution to drought risk across diverse spatial and regional contexts, all risk factors are assigned a uniform weight of 1.

2.3.8 Grading threshold

The 20th, 40th, 60th, and 80th percentiles within the data sequences (arranged from low to high) for hazard, exposure, vulnerability, sensitivity, and risk were used as the classification thresholds for the low, sub-low, moderate, sub-high, and high grades, respectively.

2.4 Identification of dominant risk factors in drought risk

The GeoDetector model, proposed by Wang and Xu (2017), is a statistical method for analyzing spatial stratified heterogeneity and identifying the underlying driving factors. It can identify interaction effects among different factors and assess their impact on the explanatory power of the dependent variables. The fundamental premise is that if an independent variable significantly influences the dependent variable, their spatial distributions should exhibit similarity. As the core component of GeoDetector, the factor detector employs the Q-statistic to quantify the relative importance of explanatory variables (Wang et al. 2016). In this study, we utilized the Optimal Parameter-based Geographic Detector (OPGD) model to identify the dominant risk factors contributing to drought disaster risk during various growth stages of maize in the Yellow River Basin (Song et al. 2020), aiming to inform the development of targeted policies and interventions.

3 Results and analysis

3.1 Analysis of maize growth stages

Based on the growth characteristics of maize, this study divided its growth cycle into five phenological stages, namely sowing-to-emergence (G1), emergence-to-jointing (G2), jointing-to-tasseling (G3), tasseling-to-milk-ripening (G4), and milk-ripening-to-maturity (G5). The sowing stage corresponds to seed placement into the soil. The emergence stage is defined when seedlings reach approximately 2 cm in height. At the jointing stage, the basal stem internodes elongate to 2–3 cm with visible tassel initiation. The tasseling stage occurs when the apical segment of the tassel is exposed (3–5 cm in length). During the milk stage, maize kernels starch deposition but remain physiologically immature. The maturity stage is characterized by kernels hardening and peak starch accumulation. Based on the core physiological processes reflected in these 5 stages, the entire growth cycle of maize can be further summarized into two main growth stages: the sowing-to-jointing stage represents the vegetative growth phase of maize, aimed at establishing a strong root system, promoting continuous leaf growth, and expanding the leaf surface area for photosynthesis. The tasseling-to-maturity stage constitutes the reproductive growth phase, dedicated to completing pollination and facilitating seed formation and maturation. Achieving equilibrium between these phases is essential for high and stable maize yields.

Based on over 20 years of maize phenological data from 54 agrometeorological stations within the study area, the spatial distribution of maize growth stages was mapped (Fig. 3). Figure 3 reveals a southeast-to-northwest increasing gradient in total maize growth duration across the Yellow River Basin, ranging from 100 to 180 days. The day of year (DOY) ranges for specific phenological stages are: sowing (DOY 89–165), emergence (DOY 112–174), jointing (DOY 160–213), tasseling (DOY 185–231), milk stage (DOY 210–261), and maturity (DOY 236–281). Notably, the temporal variability between regions progressively narrows from a 76-day range at sowing to 29 days at maturity. Spring maize in the Yellow River Basin is dominant in the upper basin, including the Shaanxi Plateau and northern Shanxi in the mid-basin region. Summer maize is mainly distributed in the mid-basin's Guanzhong Basin, southern Shanxi, and the lower basin. Based on the isotherms and isohyets in Fig. 3, the spring maize cultivation areas exhibit mean annual temperatures of 8–12 °C with < 550 mm precipitation, while summer maize areas range between 12 and 15 °C and 550–700 mm precipitation.

3.2 Characteristics of maize drought risk in the yellow river basin

3.2.1 Hazard

Figure 4 shows the spatial distribution of drought occurrence probability by intensity during critical maize growth stages in the Yellow River Basin. For the G1 stage, light drought primarily occurs in the middle-lower reaches, with probabilities ranging 0.2–0.3, and southwest Longzhong Plateau exhibits higher probability. As drought intensity increases, the areas primarily affected gradually shift northwestward. Severe drought concentrates in the upper reaches, while extreme drought is mainly in Ningxia Plain and Hetao region. During G2, light drought probability is relatively high (average 0.3 in mid-basin). Severe drought occurs mainly in areas downstream of Lanzhou (max 0.53). Extreme drought probability peaks at 0.3–0.4 in Hetao. During G3-G5, drought probabilities gradually decrease as maize matures. Light drought dominates, with shrinking spatial coverage concentrating in the upper reaches, while severe/extreme drought persist in Ningxia Plain and Hetao region.

The drought hazard for different growth stages in the Yellow River Basin was determined using Eq. (3). Figure 5 shows the highest hazard in the upper reaches, followed by the middle reaches. Hazard in the lower reaches exceeded those in the middle reaches during G1 and G5. As maize development progressed, drought hazard gradually decreased. Spatially, G1 high-hazard areas concentrated in the upper reaches, with moderate-hazard areas in the Shaanbei Plateau, Shanxi Plateau, and lower basin. For G2 and G3, high-hazard areas focused on the Ningxia Plain and Hetao region downstream of Lanzhou, while moderate-hazard areas contracted northwestward, primarily across Northern Shaanxi. During G4-G5, high-hazard areas further narrowed, concentrated in the Hetao are.

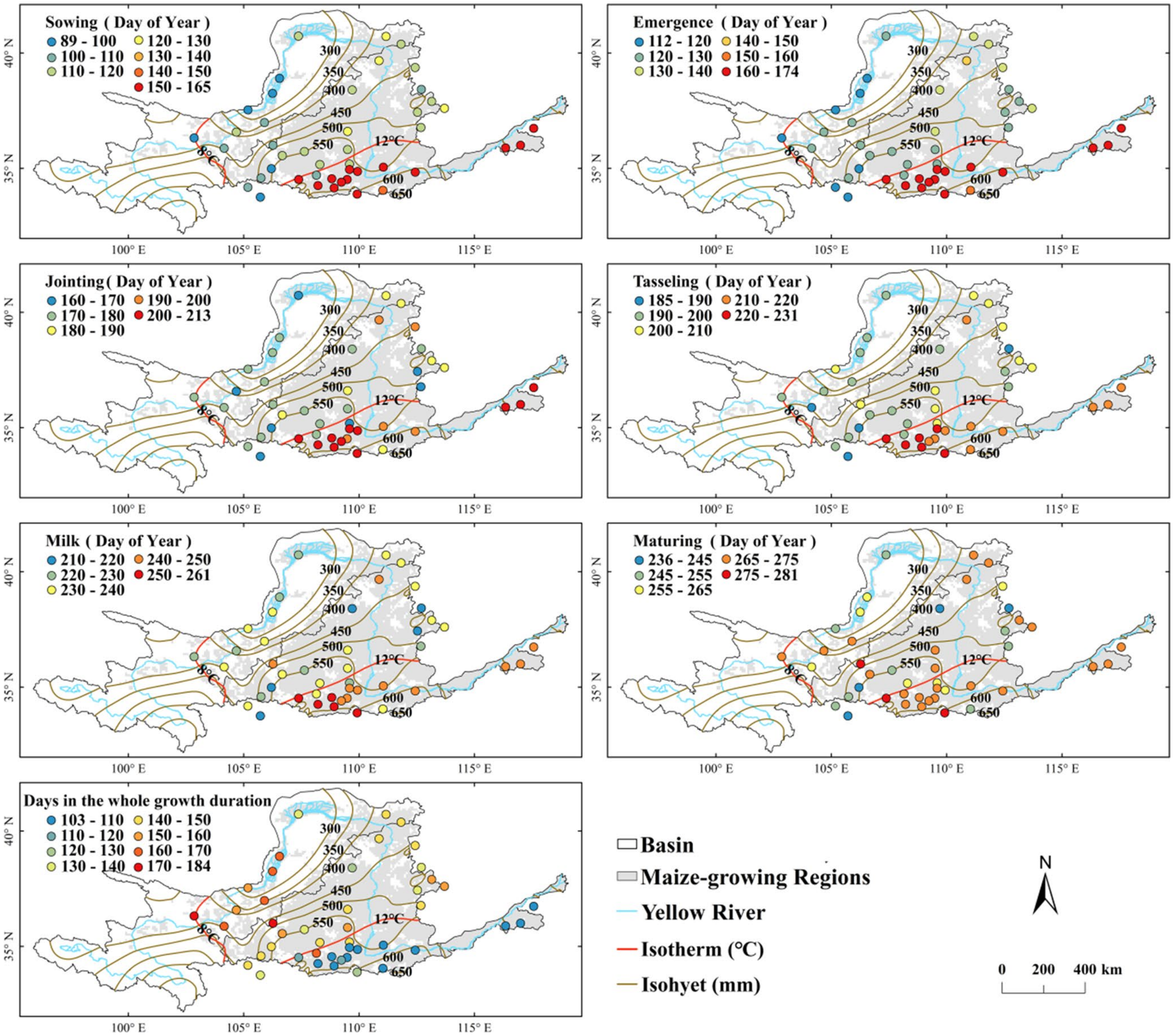

Fig. 3 Spatial distribution of DOY in maize development stages in the Yellow River Basin

3.2.2 Exposure

Figure 6 shows that areas with high maize exposure to drought were primarily located in the Ningxia Plain and Hetao Plain (upper reaches), Fenhe Plain and Guanzhong Basin (middle reaches), and North China Plain (lower reaches). Low-exposure areas concentrated in rain-fed agricultural zones of the Loess Plateau. High-exposure areas were predominantly irrigated maize systems with yields of ~18,000 kg/ha, while rain-fed maize yields ranged from 3,500 to 7,000 kg/ha.

3.2.3 Vulnerability

As shown in Fig. 7, the high-vulnerability areas for maize during the G1 stage were primarily located in the Shaanbei Plateau and the Shanxi Plateau in the middle reaches of the basin, as well as in Henan Province in the lower reaches. During the G2 stage, the high-vulnerability areas were mainly located in the Ningxia Plain in the upper reaches of the basin and in northern Shaanxi and Shanxi in the middle reaches. During the G3 stage, the areas of high vulnerability further contracted and were primarily concentrated in the Ningxia Plain in the upper reaches and central Shaanxi Province in the middle reaches. During the G4 stage, the high-vulnerability areas were primarily located in the Ningxia Plain in the upper reaches of the basin and in some

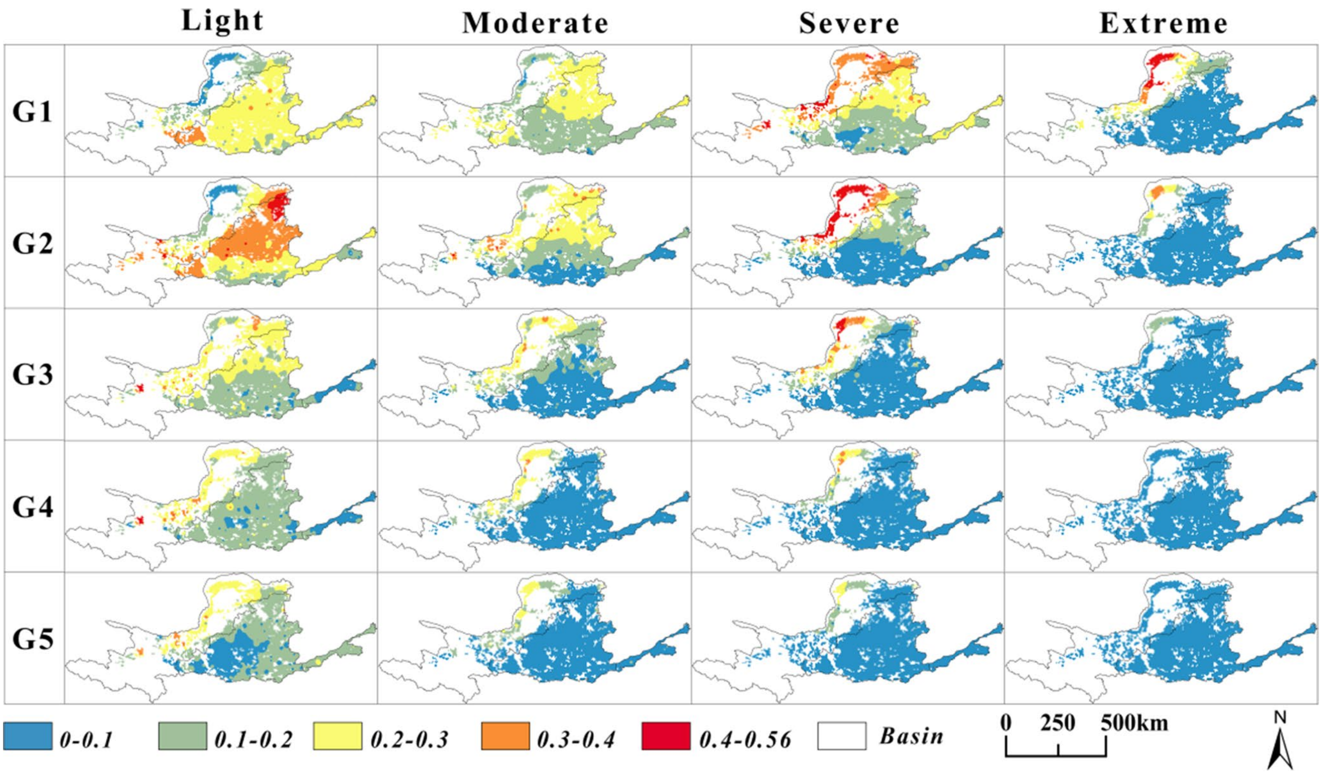

Fig. 4 Probability of drought by intensity across maize growth stages in the Yellow River Basin

parts of the downstream regions. In the G5 stage, the high-vulnerability areas were mainly found in the northern and central Shaanxi Province.

Regarding the water demand throughout the maize growth period, the water demand from sowing to emergence was the lowest, approximately 16–53 mm, accounting for 2–9% of the total water demand. The water demand from emergence to the jointing was 98–234 mm, accounting for approximately 20–42% of the total water demand. The water demand during the jointing to tasseling stage was 56–208 mm, accounting for 10–30% of the total water demand. The highest water demand occurred from tasseling to the milky stage, which was 106–250 mm, accounting for 22–41% of the total water demand. The water demand from the milky stage to maturity was 46–173 mm, accounting for 8–28% of the total water demand.

In summary, the growth period for spring maize is approximately 120–150 days, with a water demand primarily ranging between 400 and 700 mm; for summer maize, the growth period is about 90–100 days, with a water demand primarily ranging from 350 to 500 mm.

3.2.4 Sensitivity

Figure 8a illustrates that maize irrigation areas within the Yellow River Basin are primarily concentrated in the upper-reach Ningxia-Inner Mongolia Hetao Irrigation District, the middle -reach Fen-Wei Irrigation District, and the downstream Plains Yellow River Diversion Irrigation Areas. Irrigation frequency in summer maize regions exceeds that in spring maize regions; however, the total irrigation volume for summer maize is typically lower than for spring maize. As depicted in Fig. 7b, areas characterized by low plant-available soil water content are predominantly found in non-irrigated zones downstream of the Lanzhou section (upper reaches) and in the northern middle reaches. These regions are mainly covered by aeolian sandy soil, sierozem, and chestnut soil. Aeolian sandy soils exhibit high porosity and permeability but poor abilities in conserving soil/water and retaining nutrients. Due to its loose texture, low organic matter content, and week structure, sierozem exhibits poor water retention capacity. Chestnut soil features a distinct calcic layer and poor aggregate structure, resulting in low water storage capacity, characteristics that are particularly pronounced under semi-arid conditions. Regarding irrigation practices, summer maize is mainly irrigated during the sowing-to-emergence stage, with supplementary irrigation potentially applied during the mid-to-late growth stages contingent upon precipitation. In contrast, Spring maize necessitates more intensive irrigation management; timely irrigation during critical periods such as the jointing and grain-filling stages is critical for ensuring yield.

Figure 9 shows the spatial distribution of multi-year average effective precipitation across maize growth stages in the

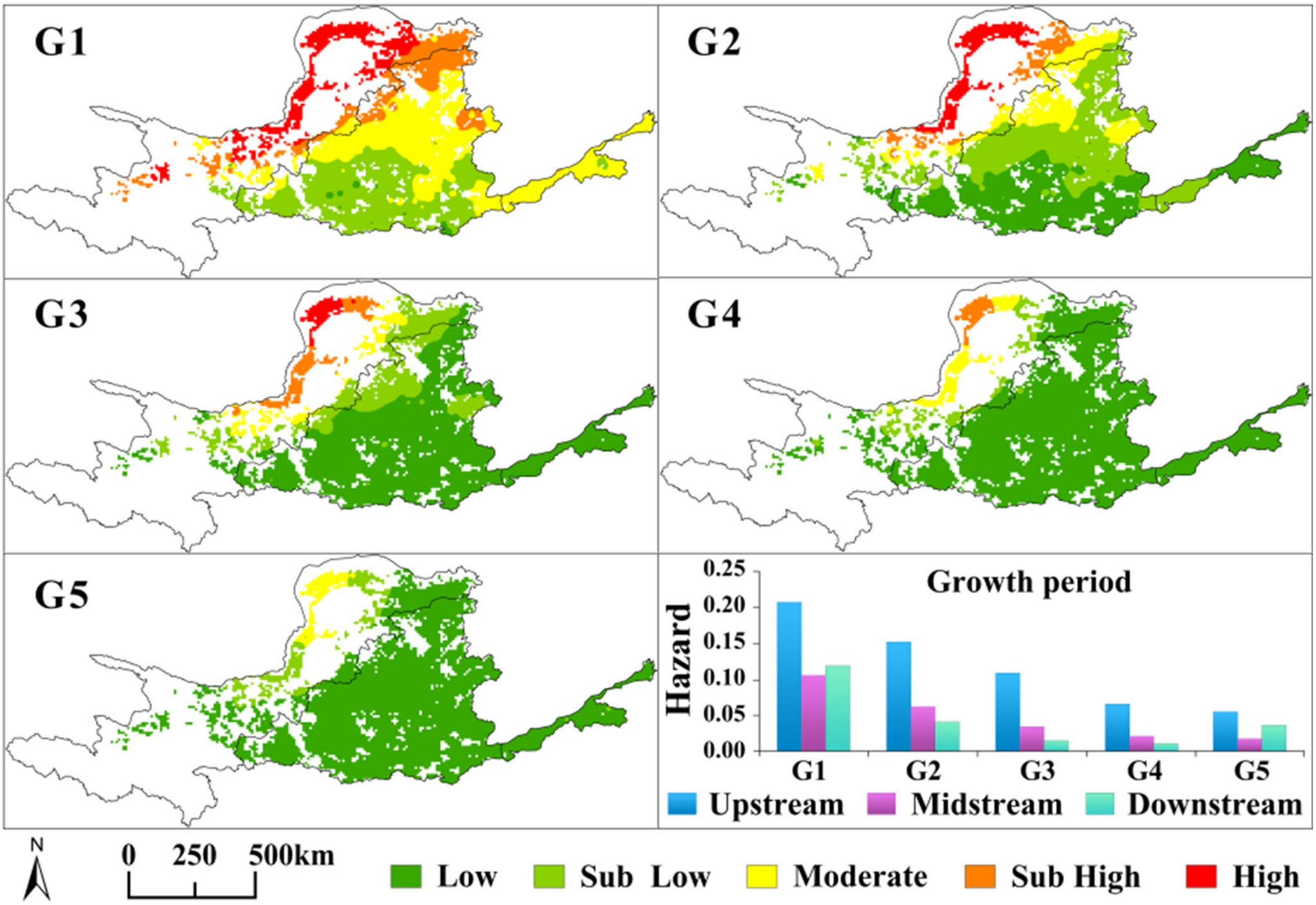

Fig. 5 Drought hazard by growth stage in the Yellow River Basin

Fig. 6 Maize drought exposure across growth stages in the Yellow River Basin

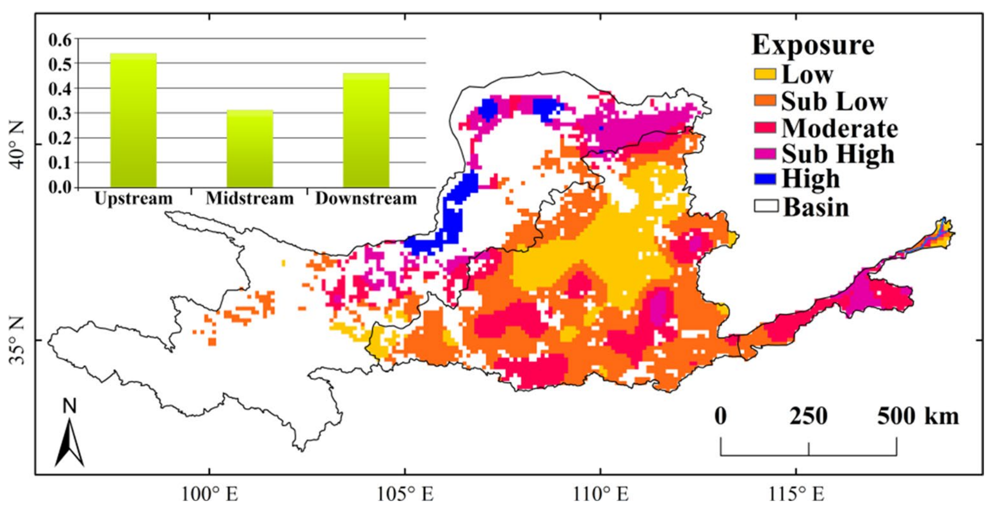

Yellow River Basin. The northeastern edge of the Qinghai-Tibet Plateau, Liupan Mountain, and Ziwuling Mountain exhibit higher effective precipitation, while the Ningxia Plain and Hetao Plain show lower values, necessitating irrigation to compensate for water deficits. As maize development progresses, the zone of higher effective precipitation exhibits a gradual extension from the southwest toward the northeast. Basin-scale analysis indicates that the average effective precipitation is 117 mm in the upper reaches, 141 mm in the middle reaches, and 133 mm in the lower reaches. The contribution of effective precipitation for each growth stage is as follows: G1 (6%), G2 (28%), G3 (18%), G4 (28%), and G5 (19%).

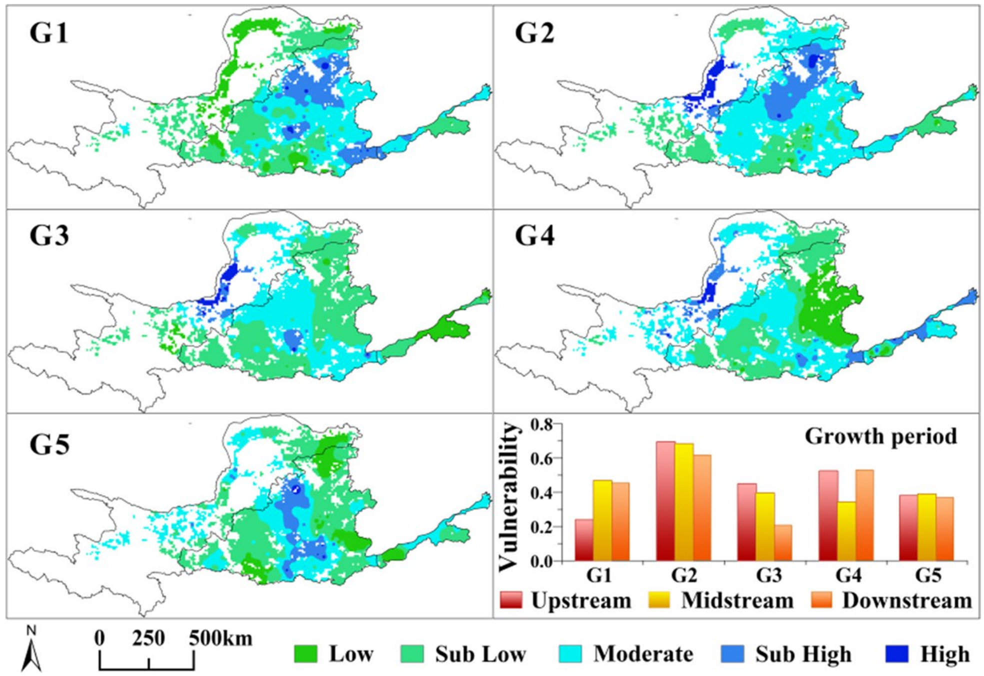

Fig. 7 Spatial distribution of maize drought vulnerability across growth stages in the Yellow River Basin

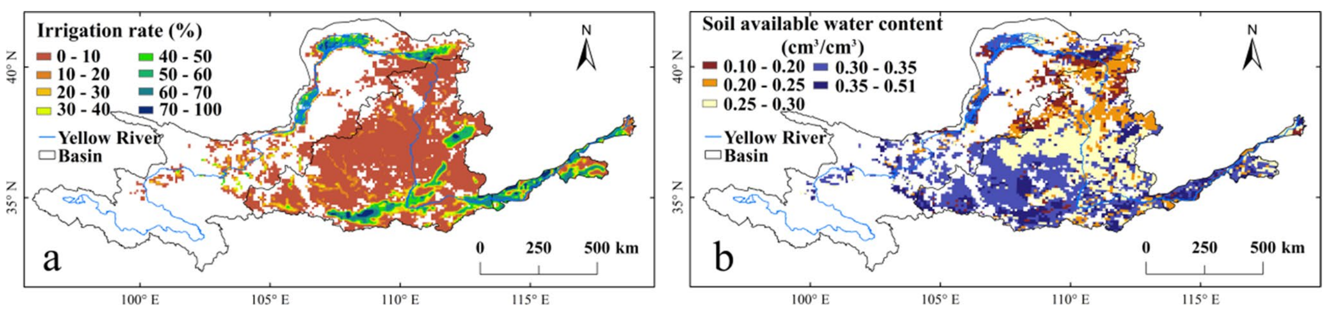

Fig. 8 Spatial distributions of (**a**) farmland irrigation ratio and (**b**) soil available water content across the Yellow River Basin

Figure 10 shows minimal variation in the overall spatial distribution of maize environmental sensitivity across growth stages. High-sensitivity zones are consistently located along the peripheries of the Mu Us, Kubuqi, and Ulan Buhe Desert, while sub-high sensitivity zones predominantly occur in the central-northern middle reaches. Low-sensitivity regions encompass the Ningxia, Hetao, and North China Plain irrigation districts; the northeastern margin of the Qinghai-Tibet Plateau; mountainous areas including the Liupan, Qinling, and Ziwuling Mountains; and the Guanzhong Basin and Fenhe Valley, with all Yellow River Basin irrigation districts exhibiting persistently low sensitivity. Basin-scale analysis shows peak sensitivity in the upper/middle reaches during stages G1 (sowing-emergence) and G4 (tasseling-milking), while the lower reaches demonstrate maximum sensitivity during stage G5 (milking-maturity), establishing a consistent sensitivity hierarchy of Upper > Middle > Lower reaches. Notably, sub-high to high sensitivity zones covered 70% of the study area during stage G4 (tasseling-milking).

3.2.5 Maize drought risk

Figure 11 shows the spatial distribution of drought risk across different maize growth stages. The high-risk zone during the G1 (sowing-emergence) was predominantly located in the Shaanbei Plateau. During the G2 (emergence-jointing), this high-risk zone expanded northwestward, covering both the Shaanbei Plateau and areas downstream of the Lanzhou section in the upper Yellow River. By the G3 (jointing-tasseling), the high-risk area contracted and became primarily concentrated in the Ningxia and Hetao Plain regions of the upper reaches. The spatial extent of high-risk areas during the G4 (tasseling-milking) remained largely consistent with G3, however, sub-high to moderate risk zones expanded significantly across the Shaanbei Plateau and Guanzhong Basin. In the G5 (milking-maturity), the high-risk area further diminished, focusing mainly on the Yinchuan-Linhe section of the upper reaches, while sub-high to moderate risk zones extended toward downstream regions. Basin-scale drought risk patterns reveal substantially elevated

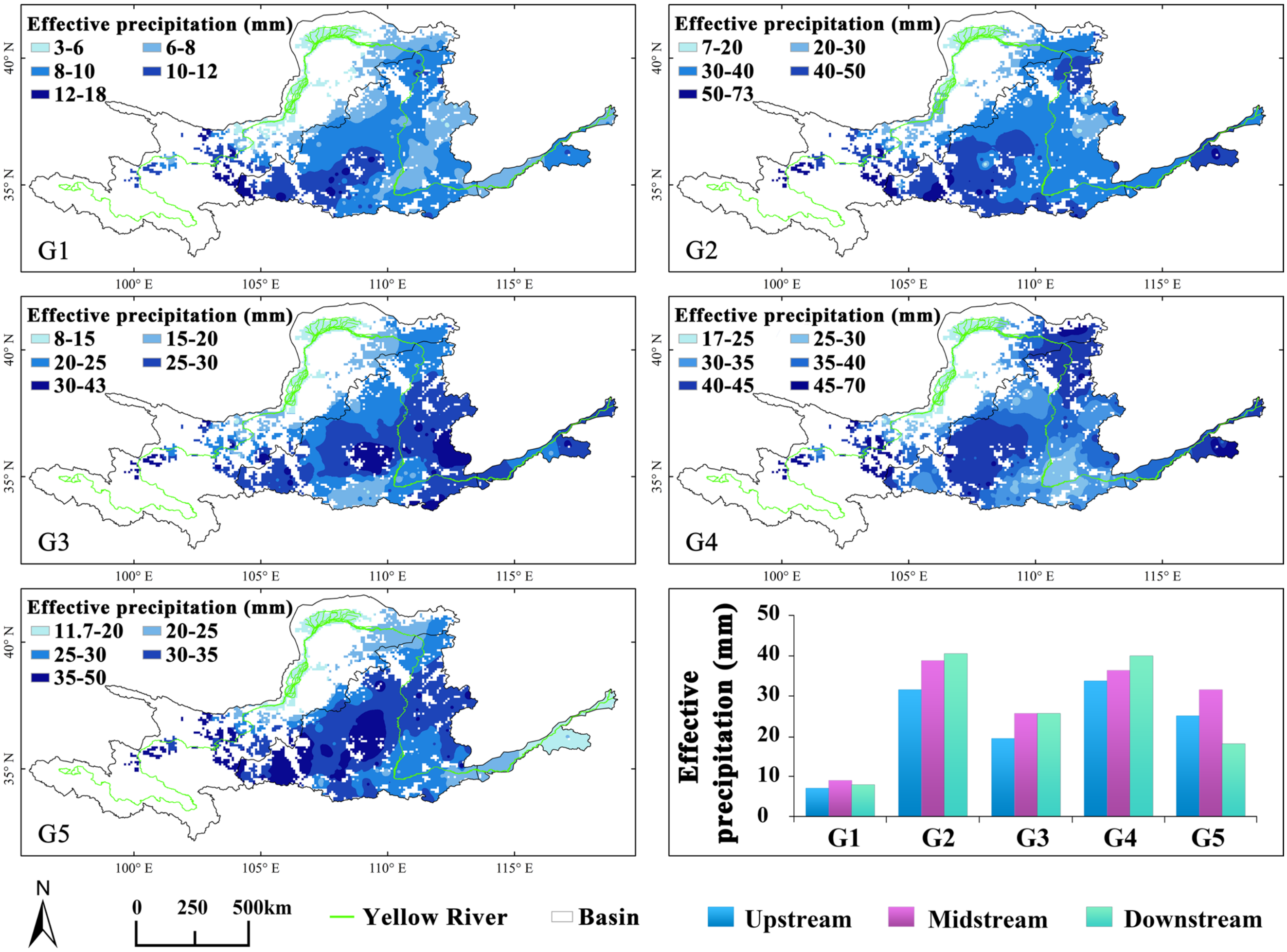

Fig. 9 Spatial distribution of effective precipitation across maize growth stages in the Yellow River Basin

risk in the upper reaches during emergence-jointing (G2) contrasted against relatively lower risk in milking-maturity (G5), while the middle reaches sustained heightened vulnerability throughout sowing-jointing (G1-G2) but demonstrated markedly reduced risk from jointing to maturity (G3-G5), and the lower reaches exhibited peak risk during both sowing-emergence (G1) and milking-maturity (G5) phases with minimal risk occurring specifically in jointing-tasseling (G3).

3.3 Dominant risk factors identified by the OPGD model for maize drought

Utilizing the OPGD model, spatial explanatory variables for drought disaster risk dynamics in maize during different growth stages were obtained. Factor detectors were then employed to quantify the contribution (Q-value) of individual risk components (Hazard, Exposure, Sensitivity, Vulnerability) to the spatial heterogeneity of drought risk, thereby identifying the dominant factors in different regions and growth stages.

It was found through the model analysis that the spatial pattern of drought risk sensitivity in the main maize production areas of the upper Yellow River reaches was predominantly associated with effective precipitation, while that in the middle and lower reaches was primarily associated with irrigation rate. Regarding the ranking of the dominant risk components based on their Q-values across growth stages (Fig. 12), the order was Hazard > Exposure > Sensitivity > Vulnerability at the G1 stage. During G2-G4 stages, the order was Hazard > Exposure > Vulnerability > Sensitivity. At the G5 stage, the dominant order was Hazard > Exposure > Sensitivity > Vulnerability.

Spatially, the model results revealed distinct patterns of dominant risk components: In the G1 stage, the hazard-dominated area was located in the upper reaches (Lanzhou-Ningxia section) and the Hetao Plain; the exposure-dominated area encompassed regions below the Lanzhou section and parts of the middle/lower reaches;

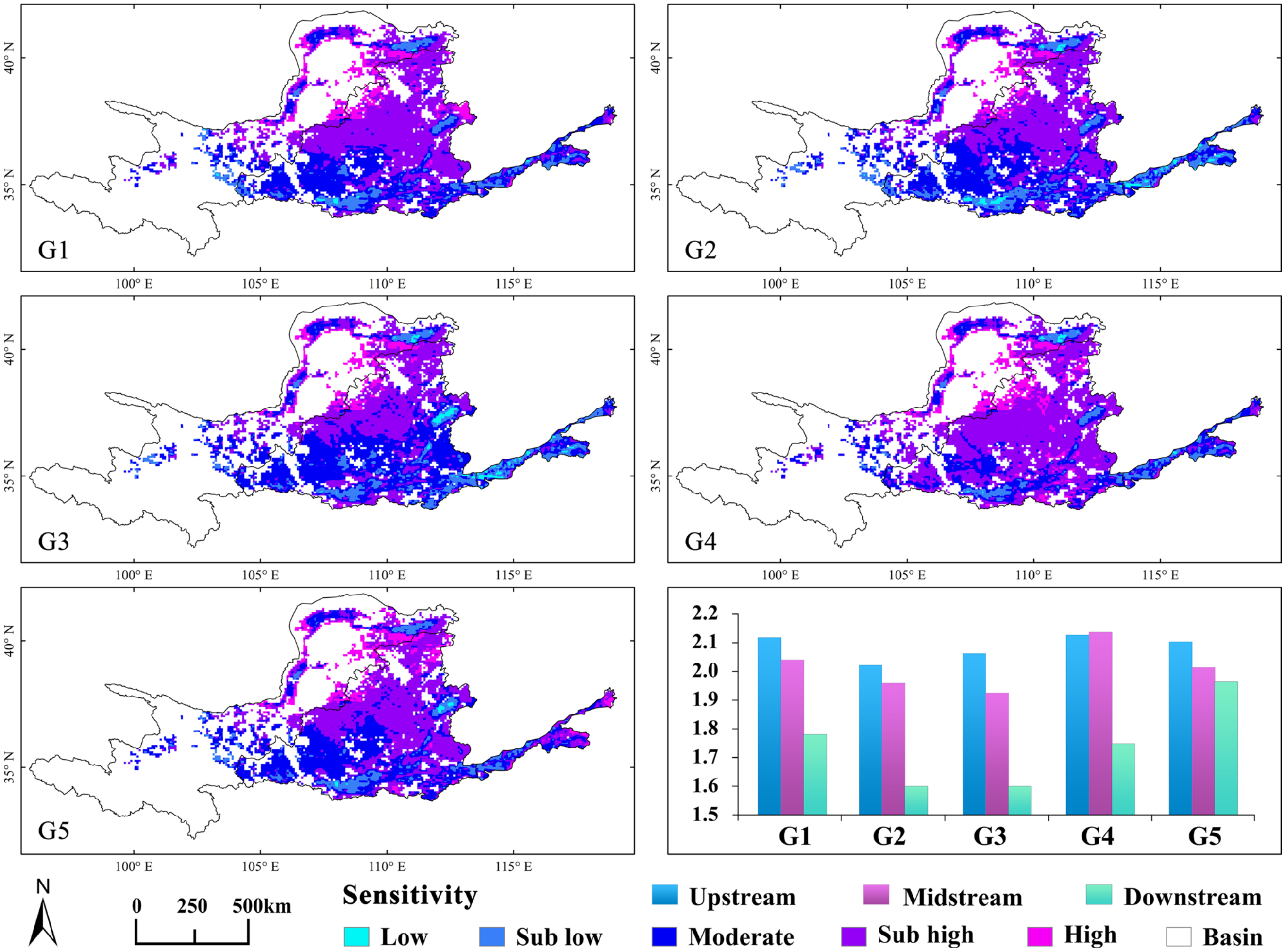

Fig. 10 Spatial distribution of environmental sensitivity across maize growth stages in the Yellow River Basin

sensitivity-dominated areas concentrated in the northwestern Shaanbei Plateau; while vulnerability-dominated areas occupied regions below the Lanzhou section and the Guanzhong Basin in the middle reaches. In the G2 and G3 stages, the hazard-dominated area was the Baotou section of the Hetao Plain, and the Ningxia Plain was co-dominated by Hazard, Exposure, and Vulnerability. In the G4 stage, the hazard-dominated area was the Linhe section of the Hetao Plain, and vulnerability dominated the Ningxia Plain. In the G5 stage, hazard continued to dominate the Linhe section of the Hetao Plain, while vulnerability dominated the western Guanzhong Plain and parts of the western Shaanbei Plateau.

Spatial interpretation indicates that drought risk in the upper reaches was primarily driven by Hazard and Vulnerability, whereas the middle/lower reaches were mainly influenced by Exposure. Overall, Hazard dominated the broad spatial distribution pattern of drought risk, while Vulnerability, Sensitivity, and Exposure shaped its localized characteristics.

Based on Fig. 12, when hazard dominates, it indicates that drought intensity/frequency exerts a significant direct impact on risk, necessitating priority improvements in disaster resistance capacity within high-hazard zones, such as constructing irrigation systems. When exposure dominates, it signifies that the spatial distribution of maize production substantially amplifies risk, requiring adjustments to planting layouts or optimization of infrastructure in high-exposure areas. When vulnerability dominates, it reflects the significant response of maize physiological stages to drought, mandating guaranteed water supply during critical growth periods. When sensitivity dominates, it demonstrates insufficient environmental resilience against drought, demanding soil improvement or selection of drought-resistant cultivars. Interaction term analysis reveals synergistic effects among risk factors; for instance, in areas jointly dominated by hazard and vulnerability, maize drought disaster risk is primarily driven by meteorological drought intensity and sensitivity during the tasseling stage.

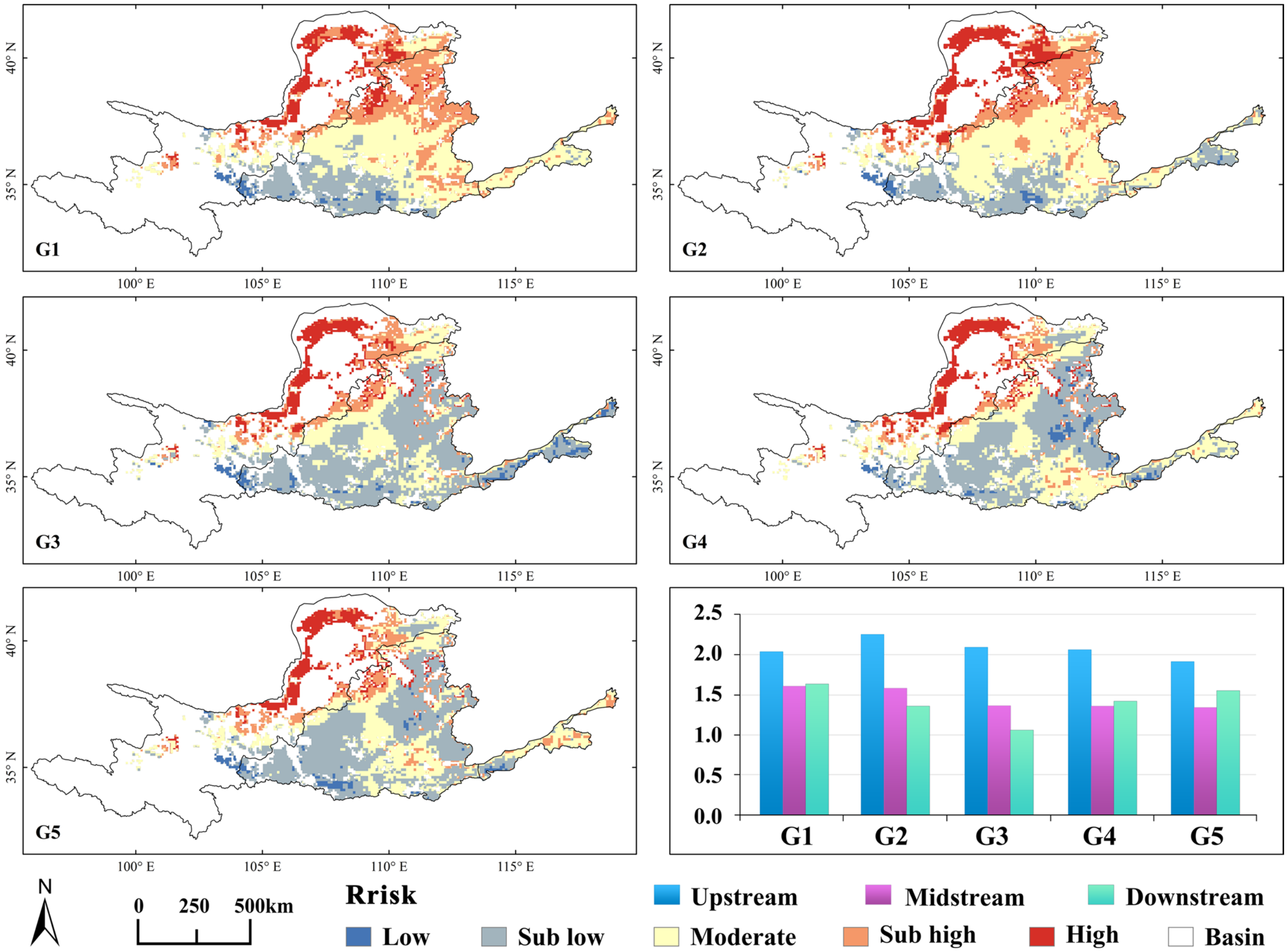

Fig. 11 Spatial distribution of drought risk across maize growth stages in the Yellow River Basin

4 Discussion and conclusion

The Yellow River Basin serves as a critical grain production base in China, benefiting from fertile soils, optimal structure, synchronized thermal-rainfall regimes, and sufficient sunshine. Maintaining stable agricultural development here is essential for national food security, regional economic growth, and ecological conservation, among other critical objectives. This study established a growth-stage-based drought disaster risk assessment framework for maize, including evaluation indices and models, identified the spatial distribution characteristics of maize drought risk over the main crop growth period, and determined the dominant risk factors using the OPGD model. The results showed that high-hazard zones for maize drought disaster in the Yellow River Basin were predominantly distributed in the upper reaches, with these zones progressively contracting southeast-northwest from stages G1 to G5. High-exposure areas concentrated primarily in irrigation districts along the Yellow River, including the Ningxia Plain, Hetao Irrigation District, Weihe Irrigation District, Guanzhong Plain, and downstream regions encompassing the Xiaolangdi Reservoir Irrigation District and Weishan Irrigation District. High-vulnerability zones clustered predominantly in the Ningxia Plain and Shaanbei Plateau, where drought vulnerability peaked during G2. High-sensitivity areas were mainly located in central-northern middle reaches, with sensitivity peaking at G4 in the upper/middle reaches and at G5 in the lower reaches. High-risk areas centered in the upper reaches and northern middle reaches, similarly contracting southeast-northwest from G1 to G5. Peak drought disaster risk periods manifested as follows: stage G2 in the upper reaches, stages G1 and G2 in the middle reaches, and stages G1 and G5 in the lower reaches.

The spatial patterns of drought vulnerability and risk in this study differed from Han et al. (2021), Ru and Ma 2022a; Shen et al. (2022a); Wang et al. (2023a). This discrepancy arises because: (1) This study focused specifically on maize, constructing indicators for crop water demand, yield, and growth-stage distribution, while others

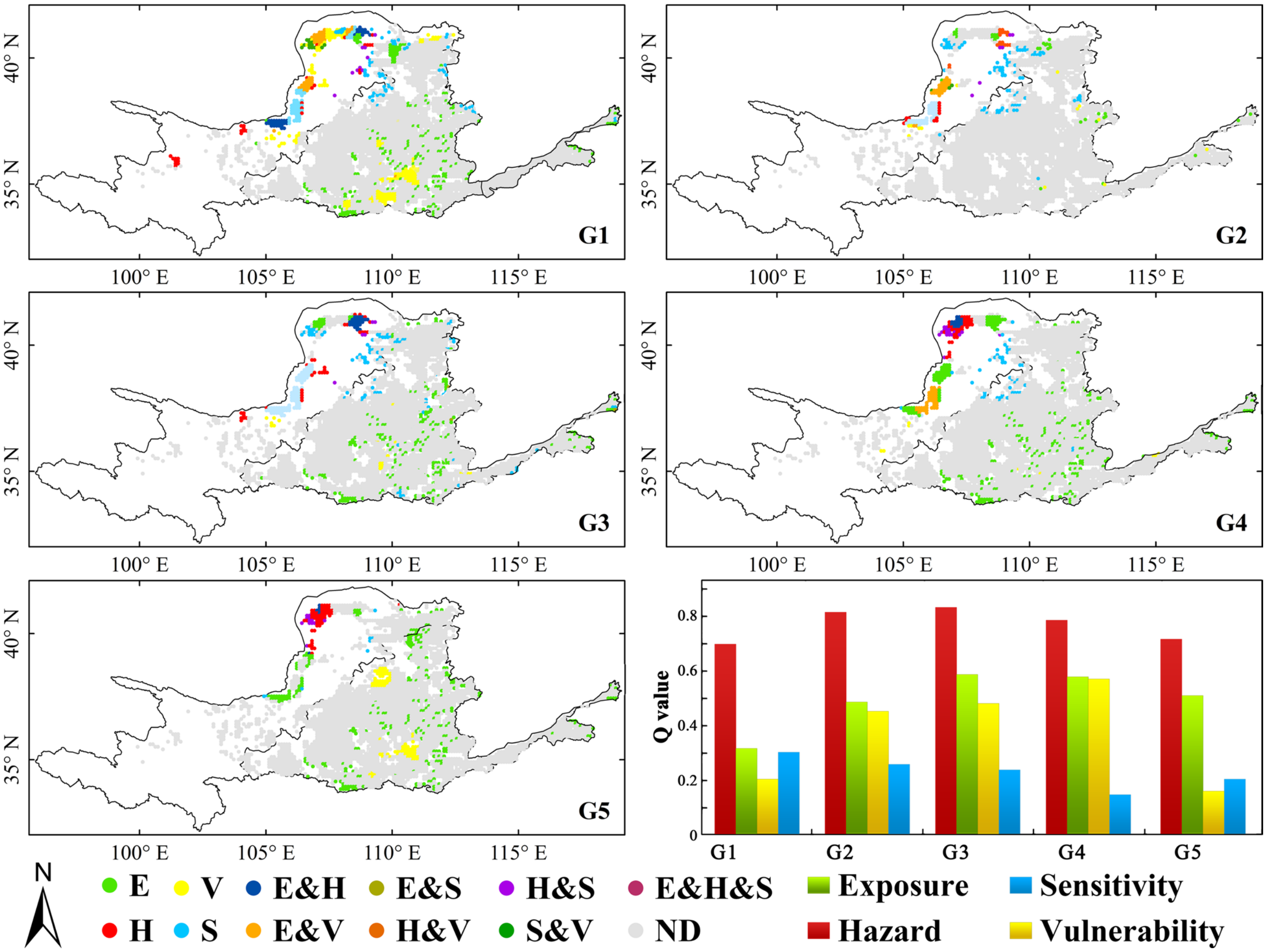

Fig. 12 Quantifying variable contributions to maize drought risk via Optimal Parameter-based Geographic Detector (OPGD) and spatial distributions of explanatory variables in the Yellow River Basin (E: Exposure, H: Hazard, S: Sensitivity, V: Vulnerability, ND: Non-significant zone)

assessed agricultural/ecological droughts at macro scales (e.g., crop area, grain yield, vegetation productivity); (2) Grid-scale analysis (this study) yields distinct results from administrative-unit-based approaches (comparison studies). This confirms that drought risk assessment must align with management objectives and spatial units to enable customized risk identification.

As a traditional agricultural region, the Yellow River Basin primarily practices rainfed agriculture and irrigated agriculture. Rainfed agriculture is predominantly found in the Loess Plateau region, where it relies heavily on natural precipitation, and droughts often lead to reduced crop yields or even crop failures. Irrigated agriculture is mainly located in riverside irrigation districts where annual precipitation is below 200 mm, and a stable water supply is essential for maintaining crop production. According to the *2022 Yellow River Water Resources Bulletin*, agricultural water use accounted for 64.7% of the total water consumption in the Yellow River Basin. Among the different river sections, the Lanzhou-Hekou reach had the highest agricultural water consumption at 12.788 billion m^3, followed by the Longmen-Sanmenxia reach (6.378 billion m^3) and the area downstream of Huayuankou (2.898 billion m^3). During severe drought events, crop irrigation demand increases while the availability of water resources for irrigation decreases. As one of the primary abiotic stress affecting maize yield, water stress (drought) can impair flowering and pollination, reduce photosynthetic efficiency, hinder nutrient uptake, and disrupt physiological metabolism, ultimately leading to reductions in both maize yield and quality (Chen et al. 2021; Ru et al. 2022b; Shen et al. 2022b). These processes ultimately manifest as "source-sink imbalance," characterized by a synchronized decline in photosynthetic product synthesis (source) and grain accumulation (sink). In our risk assessment, the high-risk levels observed during G2 (jointing–tasseling) and G5 (milking–maturity) stages macroscopically reflect this physiological mechanism—where G2 corresponds to peak sensitivity during reproductive organ differentiation, and G5 associates with the critical window for assimilate accumulation during grain filling. Therefore, effective water management practices are required to sustain high and stable maize yields in the Yellow River Basin.

Future agricultural development in the Yellow River Basin will continue to face challenges posed by climate change. Projections indicate continued temperature increases alongside greater precipitation variability, with the frequency of sub-seasonal drought events in the basin expected to rise by 23–41% – specifically manifesting as 15–30 day extensions in spring drought duration (G1–G2 stages) in the upper reaches and 20% intensity increases in summer-autumn consecutive droughts (G4–G5 stages) in the lower reaches, coupled with more frequent extreme weather events and an overall declining trend in Yellow River runoff (Li et al. 2023; Wang et al. 2024a). Research indicates that under climate warming, the joint probability of meteorological and soil drought co-occurrence in the Yellow River Basin will significantly increase. The transformation rate of meteorological drought into agricultural drought is projected to rise from the current 0.62 to 0.79, leading to more frequent vegetation drought events. Consequently, drought hazard is projected to persist with intensifying trends, exhibiting a strengthening drought cascade effect. These changes will further exacerbate maize yield loss risks due to drought (Deng et al. 2023; Wen 2024; Jia et al. 2022; Wang et al. 2024b; Kang et al. 2023). To mitigate the impacts of climate change, it is imperative to advance agricultural cultivation technologies, enhance water use efficiency in irrigation districts, and comprehensively promote agricultural water conservation throughout the basin. Key techniques include mulching for moisture retention (e.g., straw mulching), rainwater harvesting, water-saving irrigation, and the development and cultivation of drought-tolerant crop varieties. During the 14th Five-Year Plan period, the Chinese government emphasized the critical importance of agricultural water conservation. It further proposed the progressive development of digitalized irrigation district systems to achieve intelligent management and water allocation. Additionally, leveraging novel technologies such as remote sensing and deep learning, integrated with multi-source data, can improve the accuracy of agricultural water demand prediction in the basin. This advancement provides crucial technical support for water management and allocation in irrigation districts.

Utilizing surface observation data and remote sensing data, this study analyzed the distribution characteristics of drought disaster risk and dominant risk factors at different growth stages of maize in the Yellow River Basin at the grid scale. This approach facilitates decision-makers in conducting risk management based on the causes of risk. Maize drought disaster risk constitutes a complex system where risk factors are interrelated and dynamic. Consequently, establishing a comprehensive and objective risk assessment index system is highly challenging, and accurately quantifying these indicators is far from easy. In subsequent work, research on maize drought disaster risk should be further refined. Building upon data mining and collection, it is essential to systematically investigate the mechanistic characteristics of the hazard-formative environment and hazard-affected bodies within the risk transmission process, while strengthening research on maize drought resilience, sensitivity, and vulnerability. This work is of great significance for achieving a comprehensive understanding of maize drought disaster risk in the Yellow River Basin and for effectively establishing early warning and management systems for maize drought risk within the basin.

Author contributions All authors contributed to the study conception and design. Material preparation, data collection and analysis were performed by Ying Wang and Jianshun Wang. The first draft of the manuscript was written by Ying Wang and all authors commented on previous versions of the manuscript. All authors read and approved the final manuscript.

Funding This work was supported by the NSFC (Key project of National Natural Science Foundation of China) (Grant numbers 42230611), Gansu Joint Research Fund (Grant Number 25JRRA1113), Innovation and Development Project of the China Meteorological Administration (Grant Number CXFZ2024J037), Gansu Province Talent Project (Grant Number 2024QNGR33), The Third Cohort of the Longyuan Young Elites Program, Arid Land Science Research Fund (Grant Number IAM201806).

Data availability Data is provided within the manuscript files.

Declarations

Competing interests The authors declare no competing interests.

References

Allan RP (2023) Amplified seasonal range in precipitation minus evaporation. Environ Res Lett. https://doi.org/10.1088/1748-9326/acea36

Cao J, Zhang Z, Luo X, Luo Y, Xu J, Xie J, Han J, Tao F (2025) Mapping global yields of four major crops at 5-minute resolution from 1982 to 2015 using multi-source data and machine learning. Sci Data 12:357

Chen X, Liu Z, Han S, Jiang H, Xu S, Zhao H, Ren S (2021) Drought-induced reduction in photosynthesis of maize: mechanisms and implications. Agric for Meteorol 304:108412

Chen D, Guo Y, Wang R, Zhao Y, Li K, Zhang J, Liu X, Tong Z, Zhao C (2023) Quantifying multi hazards and impacts over different growth periods of maize: a study based on index construction. Int J Disaster Risk Sci 14:822–839

Chen LX, Liu JZ, Wu LZ, Shen YZ (2024) Food security: current situation, problems and countermeasures. J Agric Sci Technol. https://doi.org/10.13304/j.nykjdb.2024.0336

Cheng W, Li Y, Zuo W, Yang J, Zhang X, Zhao Q, Li L, Liu X (2024) Spatio-temporal detection of agricultural disaster vulnerability in the world and implications for developing climate-resilient agriculture. Sci Total Environ 928:172412

Deng HY, Yin YH, Zong XZ, Yin MJ (2023) Future drought risks in the Yellow River Basin and suggestions for targeted response. Int J Disaster Risk Reduct 93:103764. https://doi.org/10.1016/j.ijdrr.2023.103764

Ding Y, Zhang L, He Y, Zhang Q, Liu X, Wang J, Chen S, Li R, Zhao T (2024) Spatiotemporal evolution of agricultural drought and its attribution under different climate zones and vegetation types in the yellow river basin of China. Sci Total Environ 914:169687

FAO (1979) Yield response to water. Drainage and irrigation paper 33. FAO, Rome

Gao G, Li Y, Chen YX, Feng AQ (2023) The evolution characteristics of drought spatio-temporal law in China in the recent 30 years. China Flood Drought Manage 33(7):1–8

Han LY, Zhang Q, Ma PL, Wang YH, Huang T, Jia JY, Wang X, Wang XW, Liu WP, Li DH, Lu GY, Huang PC, Bai B (2021) Characteristics of drought disasters risk in the Yellow River Basin under the climate warming. J Desert Res 41(4):225–234

Hou M, Li Y, Biswas A, Chen X, Xie L, Liu D, Li L, Feng H, Wu S, Satoch Y, Pulatov A, Siddique KHM (2024) Concurrent drought threaten wheat and maize production and widen crop yield gaps in the future. Agric Syst 220:104056

Huang CF (2012) Risk analysis and management of natural disaster. Science Press, Beijing

Huang CF, Zhang JX, Liu J (2004) Applications of fuzzy information optimization technology. Inf Control 33(1):61–66

IPCC (2021) In: Masson-Delmotte V, Zhai P, Pirani A et al (eds) Climate change 2021: the physical science basis. Contribution of Working Group I to the Sixth Assessment Report of the Intergovernmental Panel on Climate Change. Cambridge University Press, Cambridge, UK, and New York, NY, Summary for policymakers [R]

IPCC (2023) Climate change 2023: synthesis report. Cambridge University Press. https://www.ipcc.ch/report/ar6/syr/

Jia HC, Chen F, Zhang CR, Dong JW, Du EY, Wang L (2022) High emissions could increase the future risk of maize drought in China by 60–70%. Sci Total Environ 852:158474. https://doi.org/10.1016/j.scitotenv.2022.158474

Jiang YT, Hao ZC, Feng SF, Zhang Y, Zhang X, Fu YS, Hao FH (2023) Spatiotemporal evolution characteristics in compound hot-dry events in Yangtze River and Yellow River basins. Water Resour Prot 39(2):70–77

Kang L, Wen Y, Zhou L, Chen H, Ye J (2023) Drought driving mechanism and risk situation prediction based on machine learning models in the Yellow River Basin. Geomat Nat Hazards Risk 14(1):2279493

Li Y, Huang Y, Fan J, Zhang H, Li Y, Wang X, Deng Q (2023) Meteorological and hydrological drought risks under future climate and land-use-change scenarios in the Yellow River basin. Atmosphere 14(11):1599

Liu CM, Liu XM, Tian W, Xie JX (2020) Ecological protection and high-quality development of the yellow river basin urgently need to solve the water shortage problem. Yellow River 42(9):6–9

Liu H, Zhang XL, Wang YX, Guo Y, Luo JM, Shen YJ (2021a) Spatiotemporal characteristics of the hydrothermal conditions in the growth period and various growth stages of maize in China from 1960 to 2018. Chin J Eco-Agriculture 29(8):1417–1429

Liu X, Zhang X, Wang Y, Guo Y, Luo J, Shen Y (2021b) Spatio-temporal characteristics of the hydrothermal conditions in the growth period and various growth stages of maize in China from 1960 to 2018. Chin J Eco-Agriculture 29(8):1417–1429

Liu S, Xiao L, Sun J, He P, Yang Z, van Ittersum MK (2022) Probability of maize yield failure increases with drought occurrence but partially depends on local conditions in China. Eur J Agron 139:126552

Liu K, Li X, Wang SZG (2023) Past and future adverse response of terrestrial water storages to increased vegetation growth in drylands. Npj Clim Atmospheric Sci 6(1). https://doi.org/10.1038/s41612-023-00437-9

Lu E (2009) Determining the start, duration, and strength of flood and drought with daily precipitation: rationale. Geophys Res Lett 36:L12707. https://doi.org/10.1029/2009GL038817

Ma ZG, Fu CB, Zhou TJ, Yan ZW, Li MX, Zhen ZY, Chen L, Lv MX (2020) Status and ponder of climate and hydrology changes in the Yellow River Basin. Bull Chin Acad Sci 35(1):52–60

Ma F, Zhang WJ, Feng N, Huang Y (2022) Characteristics of effective precipitation and water requirements of main crops in whole growth period in Guyuan. Res Soil Water Conserv 29(1):205–212

Meteorological Industry Standards of the People's Republic of China (2015a) Drought grade of summer maize in Northern China. QX/T, China Meteorological Press, Beijing, pp 260–2015

Meteorological Industry Standards of the People's Republic of China (2015b) Drought grade of spring maize in Northern China. QX/T, China Meteorological Press, Beijing, pp 259–2015

National Standard of the People's Republic of China (2015) Grade of agricultural drought (GB/T 32136–2015). China Standards Press, Beijing

National Standard of the People's Republic of China (2017) Grade of meteorological drought (GB/T 20481–2017). China Standards Press, Beijing

Petra D, Stefan S (2002) Global modeling of irrigation water requirements. Water Resour Res 38(4):1–8

Qin DH, Zhang JY, Shan CC, Song LC (2015) China national assessment report on risk management and adaptation of climate extremes and disasters. Science Press, Beijing

Ru SF, Ma RH (2022a) Evaluation, Spatial analysis and prediction of ecological environment vulnerability of yellow river basin. J Nat Resour 37(7):1722–1734

Ru C, Li Y, Zhang X, Wang Y, Liu X, Zhanag W, Zhao Y, Chen X, Li Y, Zhang X, Wang Y, Liu X, Zhang W, Zhao Y (2022b) Pollen viability loss under drought stress: A physiological threshold model for maize. Field Crops Res 289:108726

Shen WC, Zhang JJ, Wang K, Zhang SG, Lei HY, Song YK (2022a) Identification and differentiation of dominant ecological risks in the Loess Plateau: a case study of the middle Yellow River Basin. Acta Ecol Sin 42(18):7417–7429

Shen Y, Wang L, Zhang Q, Liu H, Li X, Chen J, Zhang Y, Wang Y, Liu Z (2022b) Nutrient transport inhibition in xylem under drought: evidence from isotopic tracing. Plant Physiol 189(3):1432–1445

Singh A, Pandey H, Pandey S, Lal D, Chauhan D, Aparna, Antre SH, Santhosh B, Kumar A (2023) Drought stress in maize: stress perception to molecular response and strategies for its improvement. Funct Integr Genomics 23:296. https://doi.org/10.1007/s10142-023-01226-6

Smith M (1992) CROPWAT – A computer program for irrigation planning and management, irrigation and drainage pap. 46, food and agric. Org. of the U. N., Rome

Song YZ, Wang JF, Ge Y, Xu CD (2020) An optimal parameters-based geographical detector model enhances geographic characteristics of explanatory variables for spatial heterogeneity analysis: cases with different types of spatial data. GIScience Remote Sens 57(5):593–610. https://doi.org/10.1080/15481603.2020.1760434

Su B, Huang J, Fischer T, Wang YJ, Kundzewicz ZW, Zhai JQ, Sun HM, Wang AQ, Zeng XF, Wang GJ, Tao H, Gemmer M, Li XC, Jiang T (2018) Drought losses in China might double between the 1.5℃ and 2.0 ℃ warming. Proc Natl Acad Sci U S A 115(42):10600–10605

UNDRR (2021) Global Assessment Report on Disaster Risk Reduction 2021: Special Report on Drought. Geneva

Wang JF, Xu CD (2017) Geodetector: principle and prospective. Acta Geogr Sin 72(1):116–134

Wang JF, Zhang TL, Fu BJ (2016) A measure of spatial stratified heterogeneity. Ecol Ind 67:260–256

Wang Q, Liu YY, Zhang YZ, Tong LJ, Li XY, Li JL, Sun ZG (2019) Assessment of spatial agglomeration of agricultural drought disaster in China from 1978 to 2016. Sci Rep 9:14393. https://doi.org/10.1038/s41598-019-51042-x

Wang Y, Wang JS, Zhang Q (2023a) Analysis of ecological drought risk characteristics and leading factors in the Yellow River Basin. Theor Appl Climatol. https://doi.org/10.1007/s00704-023-04720-w

Wang CL, Guo EL, Wang YF, Jirigala B, Kang Y, Zhang Y (2023b) Spatiotemporal variations in drought and waterlogging and their effects on maize yields at different growth stages in Jilin Province. China 118:155–180

Wang X, Li X, Shi W, Zhao H, Sun C, You S (2023c) Study on mapping of maize growth period in Huang-Huai-Hai region. Jiangsu Agric Sci 51(4):105–113

Wang BL, Wang HX, Jiao XY, Huang LT, Chen H, Guo WX (2024a) Runoff change in the Yellow River Basin of China from 1960 to 2020 and its driving factors. J Arid Land 16:168–194

Wang F, Lai HX, Wang ZP, Men R, Li Y, Jiang Y, Feng K, Tian Q, Du X, Qu Y (2024b) Dynamic relationships and propagation characteristics between meteorological drought and vegetation drought based on a three-dimensional identification algorithm. Glob Planet Change 240:104535. https://doi.org/10.1016/j.gloplacha.2024.104535

Wang JH, Lv Y, Wang J (2025) Spatio-temporal evolution characteristics of drought risk in Yangtze River Delta based on standardized precipitation index (SPI). Adv Environ Prot 15(4):668–683

Wen Q (2024) Multidimensional risk meteorological-soil joint drought (MR-MSJD) in china's crop planting. Stoch Env Res Risk Assess 38:2193–2212

Wu X, Wang PJ, Ma YP, Gong YD, Wu DR, Yang JY (2021) Standardized relative humidity index can be used to identify agricultural drought for summer maize in the Huang-Huai-Hai plain, China. Ecol Ind 131:108222

Xue R, Sun B, Li W, Wu J, Xu Y, Zhang Q, Zhang Y (2024) Future changes in compound drought events and associated population and GDP exposure in China based on CMIP6. Atmospheric and Oceanic Science Letters, p 100461

Zhang Z, Hao W, Li H, Ma L, Liu G, Wang L (2015a) Analysis on the drought characteristics in different growth stages of spring maize in Shanxi Province Chinese. J Agrometeorology 36(6):754–761

Zhang Z, Hao W, Li H, Li H, Mao L, Gao X (2015b) Analysis on the drought characteristics in different growth stages of spring maize in Shanxi Province. Chin J Agrometeorol 36(6):754–761

Zhang J, Zhang H, Chen DD, Li G, Zhang J, Zang H, Zhao Q, Hu F, Liu G, Zheng G (2020) Spatial and temporal distribution characteristics of effective rainfall and water requirement of summer maize growth period in Henan Province. J Henan Agric Sci 49(9):173–180

Zhang X, Liu K, Wang S, He Q, Liu Y, Fu B, Lv Y, Zhao P, Li Z (2022a) Spatiotemporal evolution of ecological vulnerability in the Yellow River Basin under ecological restoration initiatives. Ecol Indic 135:108586

Zhang Q, Wang Y (2022b) Distribution of hazard and risk caused by agricultural drought and flood and their correlations in summer monsoon–affected areas of China. Theor Appl Climatol. https://doi.org/10.1007/s00704-022-04093-6

Zhang Q, Li DL, Yao YB, Wang ZL, Wang Y, Wang J, Wang JS, Wang SP, Yue P, Wang H, Han LY, Si D, Li QQ, Zeng G, Wang H (2024a) Progress and prospect of the research on drought formation, prediction, and related risk assessment. Acta Meteorol Sin 82(1):1–21

Zhang S, Li M, Ma Z, Wu P, Wang H, You Q, Li J, Yin Z (2024b) The intensification of flash droughts across China from 1981 to 2021. Clim Dyn 62(5–6):3279–3295

Zhu X, Huang S, Singh VP, Zhang Q, Wang H, Leng G, Zheng X, Liu Y, Jin J (2025) Terrestrial ecosystem resilience to drought stress and driving mechanisms thereof in the Yellow River Basin, China. J Hydrol 648:9:132580